11th AIAA/ISSMO Multidisciplinary Analysis and Optimization Conference
6 - 8 September 2006, Portsmouth, Virginia

AIAA 2006-7098

DESIGNING COMPACT AND ROBUST ROCKET ENGINE COMPONENTS FOR SUSTAINABLE SPACE EXPLORATION

Man Mohan Rai[*]
NASA Ames Research Center, Moffett Field, CA-94035

ABSTRACT

Propulsion systems that are light and compact, have the necessary strength and possess robust operating characteristics are essential for space exploration. Here we explore the use of advanced design optimization methods in designing propulsion components such as turbine airfoils with these characteristics. These design methods are applied to a real world design optimization problem derived from the Space Shuttle Main Engine. The system under consideration is an axial turbine with liquid oxygen as the working fluid, the Low Pressure Oxidizer Turbo-Pump. Inspection of the first row of vanes in this turbine showed evidence of high cycle fatigue at the trailing edge near the end-walls. Several design objectives such as reduced trailing edge vortex shedding amplitude, increased airfoil strength were required to be met. Two new airfoil designs were generated using the given objectives and constraints. Here we discuss the design objectives and constraints, and the new designs. An assessment of the flow characteristics obtained for the baseline airfoil and the new designs is also provided.

INTRODUCTION

A sustainable space exploration program requires propulsion systems that are light and compact, have the necessary strength, and possess robust operating characteristics. Repair and maintenance in space can prove extremely expensive, and in some cases impractical. System redundancy as a philosophy, with its attendant cost and weight penalty, is not always a solution to the problem. In particular, if the system is susceptible to a set of operating or external conditions, having a duplicate of the same system on board is not an answer to the problem. The required component and system characteristics need to be built in at the design stage. A design process capable of such a feat will certainly be challenged by high-dimensional search spaces, multiple conflicting objectives, numerous constraints and require high fidelity, compute intensive simulation codes. Nevertheless, superior designs that reduce costs and increase reliability and safety are imperative. The advantages derived from such advanced designs, that require little or no maintenance, will not only benefit space based systems but will also result in substantial reductions in cost and system down time for earth based systems.

Fabricating and operating complex systems involves dealing with uncertainty in the relevant variables. In the case of aircraft and rocket engines, flow conditions are subject to change during operation. Efficiency and engine noise may be different from the expected values because of manufacturing tolerances and normal wear and tear. Engine components may have a shorter life than expected because of manufacturing tolerances. In spite of the important effect of operating and manufacturing uncertainty on the performance and expected life of the component or system, traditional aerodynamic shape optimization has focused on obtaining the best design given a set of deterministic flow conditions. Clearly it is important to both maintain near-optimal performance levels at off-design

---

American Institute of Aeronautics and Astronautics

operating conditions, and, ensure that performance does not degrade appreciably when the component shape differs from the optimal shape due to manufacturing tolerances and normal wear and tear. These requirements naturally lead to the idea of robust optimal design wherein the concept of robustness to various perturbations is built into the design optimization procedure.

Recognition of the importance of incorporating the probabilistic nature of the variables involved in designing and operating complex systems has led to a few investigations in the recent past. Some of the basic principles of robust optimal design are discussed by Egorov et al.[1]. Several commonly used approaches such as maximizing the mean value of the performance metric, minimizing the deviation of this metric and, maximizing the probability that the efficiency value is no less than a prescribed value are discussed in their paper. Egorov et al.[1] make the observations that a) robust design optimization is in essence multi-objective design optimization because of the presence of the additional objective (robustness) and, b) the addition of the robustness criterion may result in an optimal solution that is substantially different from that obtained without this criterion. Various approaches to robust optimal design are also mentioned in this article.

While the discussion above focused on the effect of uncertainty in the variables on performance, their effect on constraint satisfaction is equally important from a reliability perspective. Here the focus is on maximizing the probability of constraint satisfaction. Koch et al.[2], provide a discussion of this and related concepts. Some of the basic steps involved in both robust optimal design as well as reliability-based optimization such as a) identifying random variables and their associated probability density functions, b) reducing this set of variables to a smaller subset of key random variables, to reduce optimization costs and, c) the effective utilization of Monte Carlo techniques to obtain estimates of performance variability or reliability, are discussed by the authors.

Simulation based design optimization can be computationally expensive in cases where the underlying physics is complicated. Some of the contributing factors are three-dimensionality, a large disparity in the largest and smallest scales that are required for an accurate analysis etc. The addition of the robustness criterion can greatly increase computational requirements because of the need to estimate the variance in performance or reliability. Koch et al.[2], reduce computational cost by first obtaining the optimal solution via a deterministic approach and subsequently adding the reliability requirement. In a separate article Koch et al.[3] use Kriging models to compute performance variability and reliability.

The imposition of the additional requirement of robustness results in a multiple-objective optimization problem requiring appropriate solution procedures. Typically the costs associated with multiple-objective optimization are substantial. Efficient multiple-objective optimization procedures are crucial to the rapid deployment of the concepts of robust design.

Single- and multiple-objective objective optimization methodologies based on artificial neural networks and evolutionary algorithms have been in development over several years at NASA ARC [4- 8]. The network-based design optimization codes utilize hybrid neural networks to model the behavior of any objective in design space. The models are then used to search for optimal designs. The goal here is to reduce the number of simulations required to obtain the optimal design. The network models serve as surrogates to the simulation codes. The work in algorithm development focuses on seeking ways to reduce the number of simulations required to develop accurate models in high-dimensional design spaces, to improve the generalization ability of neural networks in both the interpolative and extrapolative modes via advanced training algorithms and, to develop an integrated design system that utilizes the power of parallel computing. In a parallel effort a design optimization system based on the method of Differential Evolution[9] (DE) is also being developed. The algorithmic goals here are to reduce the population sizes, and the number of generations required to obtain the global optimum. The more practical goal is a significant decrease in cost to solution. More recently these methods have been extended to robust optimal design where performance insensitivity to manufacturing tolerances, normal wear and tear, and random disturbances in operating conditions is an additional objective. Considerable progress in the effective extension of DE to multiple-objective optimization has been achieved[8].

Here we apply the methodology[4-8] to a real world design optimization problem derived from the Space Shuttle Main Engine (SSME). The system under consideration is an axial turbine with liquid oxygen as the working fluid, the Low Pressure Oxidizer Turbo-Pump (LPOTP). Inspection of the first row of vanes in this turbine showed evidence of high cycle fatigue at the trailing edge near the end-walls. CFD analysis of the known sources of HCF indicated vortex shedding as the most probable cause[10]. It was found that the shedding frequency range overlapped the vane trailing edge flapping mode natural frequency. At the present time the first vane of the LPOTP is replaced at carefully monitored time intervals thus ensuring the safety of the Shuttle flights[10]. A first attempt at redesigning the vane is reported in Ref. 10. The objectives pursued were increased vane strength, decreased shedding amplitude, decoupling of the shedding and vane natural frequencies, minimal impact on downstream rows and, robustness to manufacturing tolerances. The design assessment reported in Ref. 10 indicated that all of these objectives were achieved in substantial measure. *Here, we redesign the vane to make it lighter in weight and more compact. All of the original objectives and constraints are retained.*

Trailing edge vortex shedding is a complex phenomenon that depends on the Reynolds number, the nature of the suction and pressure side boundary layers, the shape of the trailing edge and other factors. Hence Ref. 10 presents results obtained from four different codes and turbulence models for the baseline and optimized airfoils. All of these codes solve the Reynolds Averaged Navier-Stokes (RANS) equations in conjunction with various turbulence models to provide time accurate simulations of the flow through the LPOTP turbine. While these turbulence models have been validated for several classes of flows over a period of years, their ability to accurately model turbulence in the context of vortex shedding in LOX has not been investigated. The complexities of shedding and limitations of the turbulence models must be kept in mind in evaluating the results presented in Ref. 10. The persistence of laminar-like vortex streets several trailing edge diameters downstream of the vane in the computations and the ability of the codes to model the effects of surface boundary layer turbulence on shedding characteristics are of some concern. Direct numerical simulations (DNS) and detailed experiments are required to fully understand trailing edge vortex shedding. A remarkable finding in Ref. 10 is that all of the codes and corresponding turbulence models indicate essentially the same qualitative trends in flow quality and significant performance improvements for the redesigned airfoil. Here as in Ref. 10, RANS simulations using a turbulence model are used for preliminary assessment of the shedding phenomenon.

AIRFOIL REDESIGN AND PRELIMINARY ASSESSMENT

The optimized airfoils and preliminary flow assessments of the baseline airfoil, the optimized airfoil of Ref. 10 (referred to as O5) and the optimized airfoil developed in this study (referred to as O6) are presented in this section. Flow computations are performed using the code ROTOR-2 [11,12] and the Baldwin-Lomax turbulence model (one of the models used in Ref. 10). The flow is assumed to be turbulent on both the pressure and suction sides of the airfoil because of the high disturbance levels in the operating environment (private communication, Dr. B. Marcu, Pratt & Whitney Rocketdyne).

A comparison of the baseline and O5 airfoils

The first redesign of the baseline airfoil (baseline is from the LPOTP of the SSME) is discussed in Ref.10. The detailed design requirements are also provided there and are outlined below:

- Increase the thickness of the airfoil, particularly in the trailing edge region, to both strengthen the airfoil and increase its natural frequency corresponding to the trailing edge flapping mode
- Reduce trailing edge vortex shedding amplitude
- Decrease trailing edge vortex shedding frequency to obtain greater separation of frequencies (shedding and natural flap mode frequencies)
- Maintain throat area

- Maintain exit flow angle
- Design a trailing edge that eases the manufacturing process (facilitate metal flow in casting)
- Reduce pressure fluctuations on downstream airfoil rows
- Desensitize shedding amplitude to manufacturing tolerances and normal wear and tear

The last requirement was added because the preferred manufacturing technique is casting, with a large manufacturing tolerance of ± 0.006 inches. Thus the variation of the baseline trailing edge geometry because of manufacturing tolerances is substantially more than 50%. Consequently, any attempt to redesign the trailing edge to minimize the shedding amplitude must include the principles of robust optimal design.

The baseline airfoil and optimized airfoil (referred to as O5) from Ref. 10 are shown in Fig. 1. Clearly the new airfoil is thicker and stronger. A stress analysis of the baseline and O5 airfoils showed that all relevant measures of stress were lower for O5. The corresponding increase in safety factors for O5 ranged from 3.5 to 6.3. It was concluded in Ref. 10 that the part fitted with the O5 airfoil possessed an essentially infinite life in operation.

Figure 2 shows the time-averaged pressure distributions on the baseline and O5 airfoils. Clearly there is a redistribution of the load. The loading on O5 is more uniform. In particular, the loading at the leading edge is higher for O5 than the baseline. Additionally in the last quarter chord, where both the airfoils are leaner, O5 shows a smaller load than the baseline. Figure 3 shows the surface pressure amplitudes for the two airfoils (unsteady loads caused by trailing edge vortex shedding). The amplitude distribution obtained with O5 is lower than that obtained with the baseline airfoil on the entire airfoil surface. In particular, O5 shows a reduction of 75% in peak amplitude (this occurs on the pressure side of the trailing edge).

Figure 4 shows the time variation of the surface pressure on O5 and the baseline airfoil at the point of maximum fluctuating pressure amplitude. This point occurs on the pressure side of the trailing edge for both airfoils. The decrease in amplitude obtained with O5 is clearly visible here. It can also be observed that O5 yields a lower shedding frequency. Figure 5 shows results obtained from a spectral analysis of the waveforms in Fig. 4. Again, the reduction in amplitude obtained with O5 is clearly visible. It can also be seen that the baseline airfoil sheds at a frequency of 48.6 Kilohertz and O5 sheds at 37.8 Kilohertz. Thus O5 results in a reduction of 22% in shedding frequency. Based on extensive structural dynamics analyses reported in Ref. 10 it was concluded there that, this reduction in shedding frequency coupled with an increase in the flapping mode natural frequency (for O5) results in a complete detuning of the two frequencies.

Unsteady rotor-stator computations including the first row of stators (baseline or O5 airfoils), the downstream rotor row and, the second stator row (downstream of the rotor row) are also presented in Ref. 10. These computations show that replacing the baseline airfoils in the first row with the O5 airfoils results in a modest improvement   or, no change, in the flow downstream. *In conclusion, the results of Ref. 10 demonstrate that all of the objectives of the optimization effort were met*.

A comparison of the baseline and O6 airfoils

As seen in Fig. 1, O5 is much larger than the baseline airfoil. One objective that was not included earlier was compactness. The following questions come to mind when reviewing the design and assessment exercise described in Ref. 10. Is it possible to design an airfoil that is substantially thicker than the baseline in the trailing edge region (second half of the airfoil) and yet have the leading edge dimension approximately the same? Is it possible to shorten the airfoil and thus obtain a redesign that is lighter and stronger than the baseline? Is it possible to achieve these goals while simultaneously meeting all of the objectives of Ref. 10 (mentioned earlier)? The current effort focuses on obtaining a design that achieves all of these goals.

4

The shape of the newly designed airfoil (O6) is compared to the baseline airfoil in Fig. 6. Note that O6 has been masked by a nonlinear transform (pending approval from NASA ARC to publish the actual airfoil shape). It is shorter than the baseline, has approximately the same leading edge dimension but is thicker than the baseline in the last 65% of the axial chord. The interior volume per unit span, and thus the weight, of O6 is about 92.8% of that obtained for the baseline airfoil. The corresponding value for O5 is about 151% of the baseline value. A comparison of Figs. 1 and 6, which are drawn to the same scale, shows that O6 is considerably smaller than O5.

The time-averaged surface pressure distributions for the baseline and O6 airfoils are shown in Fig. 7. Although the axial chord of O6 is smaller than that of the baseline, the pressure distributions are plotted as a function of the axial position normalized by the axial chord (c) and, are thus of the same extent in this figure. The leading edge load is much higher for O6. In fact, O6 loading is almost uniform to about 65% axial chord and then diminishes near the trailing edge. This higher loading is required to achieve the necessary turning and flow acceleration over a shorter axial distance. On the other hand, the baseline has almost no load at the leading edge and peak loading at about 75% axial chord. Figure 8 shows the surface pressure amplitudes for O6 and the baseline airfoil. The amplitude distribution obtained with O6 is lower than that obtained with both the baseline airfoil and O5 (compare Figs. 3 and 8) on the entire airfoil surface. In particular, O6 shows a reduction of 90% in peak amplitude (which occurs on the pressure side of the trailing edge). In this aspect O6 is an improvement over both O5 and the baseline airfoil.

Figure 9 shows the time variation of the surface pressure on O6 and the baseline airfoils at the point of maximum fluctuating pressure amplitude. This point occurs on the pressure side of the trailing edge for both airfoils. The decrease in amplitude obtained with O6 is clearly visible here. It can also be observed that O6 yields a lower shedding frequency. Figure 10 shows results obtained from a spectral analysis of the waveforms in Fig. 9. Again, the substantial reduction in amplitude obtained with O6 is observed. It can also be seen that the baseline airfoil sheds at a frequency of 48.6 Kilohertz and O6 sheds at 40.5 Kilohertz. Thus O6 results in a 17% reduction in shedding frequency. This reduction is a little lower than the obtained for O5 (peak at 37.8 Kilohertz). The natural flapping mode frequency has not yet been determined but is anticipated to be close to that of O5 because of increased airfoil thickness in trailing edge region.

As mentioned earlier, the choice of manufacturing method can have a considerable effect on shedding characteristics. Casting, with manufacturing tolerances of ± 0.006 inches (resulting in the trailing edge geometry varying by substantially more than 50%), could easily result in a complete loss of any optimal shedding characteristics that are obtained via design optimization. Both O5 and O6 were designed to maintain low shedding amplitudes even in the presence of manufacturing tolerances as large as ± 0.006 inches. As a part of the assessment process, several random perturbations of O6 were generated using the geometry perturbation method described in Ref. 8. These perturbations were generated so the maximum variation in shape in a direction normal to the airfoil surface was less than or equal to 0.006 inches in magnitude.

Figure 11 shows four of these random perturbations (P1, P2, P3 & P4) together with O6. The perturbations in shape are clearly visible. A detailed examination of the trailing edge region shows opposite trends for the airfoils P1 and P4. P1 is thicker and P4 is thinner than O6 everywhere in this region. The airfoils P2 and P3 also exhibit opposite trends. P2 is thinner on the pressure side and thicker on the suction side of the trailing edge while P3 is thinner on the suction side and thicker on the pressure side of the trailing edge. The airfoils P1 – P4 were chosen out of several randomly generated perturbations because of the different trends they represent. Flow computations were then performed for all of them using ROTOR-2. Figure 12 shows the pressure amplitude distributions for O6, P1, P2, P3, P4 and the baseline airfoil. The amplitude distributions obtained with the perturbed airfoil shapes are different. However, on the scale of the peak value obtained for the baseline, all of the peak amplitude values (P1 – P4) are about the same as that obtained for O6. This is a strong indication that shedding amplitude insensitivity to perturbations in airfoil shape was achieved during design optimization. The four perturbations of O6 are only a small subset of all the possible perturbations that can be generated during

American Institute of Aeronautics and Astronautics

the manufacturing process. Thus the data obtained for these four cases serve as an indicator of robust performance but do not confirm it for all possible deviations in shape.

The trailing edge of O6 is larger than the baseline trailing edge and completely encompasses the latter. Thus it is expected to be easier to manufacture than the baseline. Additionally, the throat area and flow exit angle for both O5 and O6 are very nearly the same as for the baseline. The results presented thus far, demonstrate that all of the objectives mentioned earlier have been achieved except for one, i.e., the effect on downstream airfoils. A stator-rotor simulation for O6 will be provided in a separate article. However, it is anticipated that because of the lower shedding amplitude exhibited by O6, there will be a small gain in overall system performance (smaller unsteady forces on the rotor).

As mentioned earlier, trailing edge shedding is a complex phenomenon that is dependent on a number of factors. The approach taken in Ref. 10 in assessing O5 was to use multiple turbulence models. Since all of the turbulence models used in Ref. 10 indicated a substantial reduction in shedding amplitude this exercise was not repeated here. A true understanding of the trailing edge flow can only be obtained via a comprehensive experiment or a Direct Numerical Simulation (DNS) of the flow. A first step in this direction is reported in Ref. 13 where a DNS of flow over a turbine airfoil and the associated numerical methodology are presented. Direct numerical simulations of the flow over the baseline, O5 and O6 airfoils are currently being planned. These simulations should resolve any existing doubts of the validity of the reduction in shedding amplitudes that has been achieved and aid in understanding the physical mechanisms underlying the observed data from the RANS computations.

SUMMARY

Propulsion systems that are light and compact, have the necessary strength and possess robust operating characteristics are essential for space exploration. Here we explore the use of advanced design optimization methods in designing propulsion system components such as turbine airfoils with these characteristics. These design methods are applied to a real world design optimization problem derived from the Space Shuttle Main Engine. The system under consideration is an axial turbine with liquid oxygen as the working fluid, the Low Pressure Oxidizer Turbo-Pump. Inspection of the first row of vanes in this turbine showed evidence of high cycle fatigue at the trailing edge near the end-walls. Earlier CFD analysis of the known sources of HCF indicated vortex shedding as the most probable cause.

Several design objectives such as reduced trailing edge vortex shedding amplitude, increased airfoil strength etc. were required to be met. Two new airfoil designs were generated using the given objectives and constraints. Here we discuss the design objectives and constraints, and the new designs. An assessment of the flow characteristics obtained for the baseline airfoil and the new designs is also provided. The assessments provided here and in a related earlier publication[10] demonstrate that the two new airfoils meet the design objectives. The downstream effects caused by O6 are yet to be determined but it is anticipated that the unsteady forces on the downstream rotor will be nearly the same or slightly smaller than those obtained with O5 and the baseline. In addition O6 is lighter and more compact than both the baseline and O5. One significant achievement of both Ref. 10 and the current design effort is the desensitization of the shedding amplitude to large changes in trailing edge shape.

Although the redesigned airfoils presented here are of practical interest in their own right, an important contribution of this paper is the demonstration that design processes of the kind utilized in this study can be used to significantly improve component strength, reliability and operational robustness and thus enhance safety and reduce lifetime costs. Furthermore these goals may be achieved even in the presence of multiple conflicting objectives and numerous constraints.

REFERENCES

1. Egorov, I. N., Kretinin, G. V., and Leshchenko, I. A., "How to Execute Robust Design," AIAA Paper No. 2002-5670, 9th AIAA/USAF/NASA/ISSMO Symposium on Multidisciplinary Analysis and Optimization, September 4-6, Atlanta, Georgia.

2. Koch, P. N., Wujek, B., Golovidov, O., "A Multi-Stage, Parallel Implementation of Probabilistic Design Optimization in an MDO Framework," AIAA Paper No. 2000-4805, 8th AIAA/USAF/NASA/ISSMO Symposium on Multidisciplinary Analysis and Optimization, Long Beach, California.

3. Koch, P. N., Wujek, B., Golovidov, O., and Simpson, T. W., "Facilitating probabilistic multidisciplinary Design Optimization Using Kriging Approximation Models," 9th AIAA/USAF/NASA/ISSMO Symposium on Multidisciplinary Analysis and Optimization, September 4-6, Atlanta, Georgia.

4. Rai, M. M., "A Rapid Aerodynamic Design Procedure Based on Artificial Neural Networks," AIAA Paper No. 2001-0315, AIAA 39th Aerospace Sciences Meeting, Reno, Nevada, Jan. 8-11, 2001.

5. Rai, M. M., "Three-Dimensional Aerodynamic Design Using Artificial Neural Networks," AIAA Paper No. 2002-0987, AIAA 40th Aerospace Sciences Meeting, Reno, Nevada, Jan. 14-17, 2002.

6. Rai, M. M., "Towards a Hybrid Aerodynamic Design Procedure Based on Neural Networks and Evolutionary Methods," AIAA Paper No. 2002-3143, AIAA 20th Applied Aerodynamics Conference, St. Louis Missouri, June 24-26, 2002.

7. Rai, M. M., "Robust Optimal Aerodynamic Design Using Evolutionary Methods and Neural Networks," AIAA Paper No. 2004-0778, AIAA 42nd Aerospace Sciences Meeting, Reno, Nevada, Jan. 5-8, 2004.

8. Rai, M. M., "Robust Optimal Design With Differential Evolution", AIAA Paper No. 2004-4588, Tenth AIAA/ISSMO Multidisciplinary Analysis and Optimization Conference, Albany, New York, August 30th – September 1st, 2004.

9. Price, K., and Storn, N., "Differential Evolution," *Dr. Dobb's Journal*, April 1997, pp. 18-24.

10. Marcu, B., Hadid, A., Lin, P., Balcazar, D., Rai, M. M., and Dorney, D. J., "Towards Rocket Engine Components With Increased Strength and Robust Operating Characteristics," 41st AIAA/ASME/SAE/ASEE Joint Propulsion Conference & Exhibit, Tucson, Arizona, July 10-13, 2005.

11. Rai, M. M., "Navier-Stokes Simulations of Rotor-Stator Interaction Using Patched and Overlaid Grids," AIAA *Journal of Propulsion and Power*, Vol. 3, No. 5, September-October 1987, pp. 387-396.

12. Rai, M. M., and Madavan, N. K., "Multi-Airfoil Navier-Stokes Simulations of Turbine Rotor-Stator Interaction," *ASME Journal of Turbomachinery* , Vol. 112, No. 3, July 1990, pp. 377-384.

13. Rai, M. M., "Direct Numerical Simulation of Transitional and Turbulent Flow on a Turbine Airfoil," AIAA Paper No. 2006-4460, 42rd AIAA/ASME/SAE/ASEE Joint Propulsion Conference, Sacramento, California, July 9 – 12, 2006.

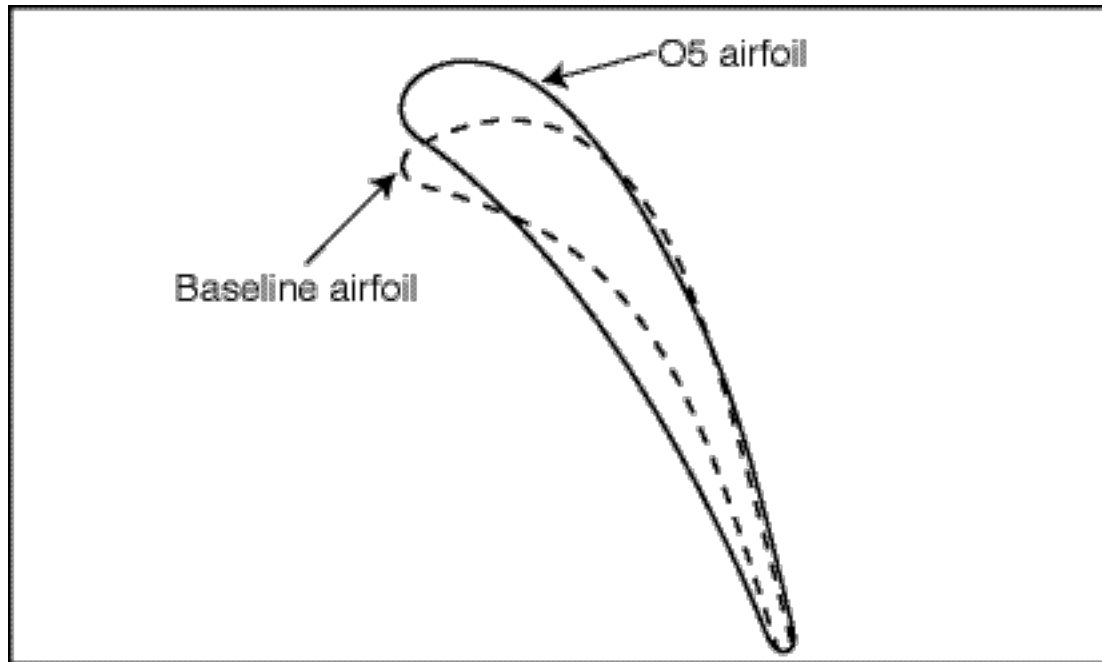American Institute of Aeronautics and Astronautics

Figure 1. A comparison of the baseline and O5 airfoil shapes.
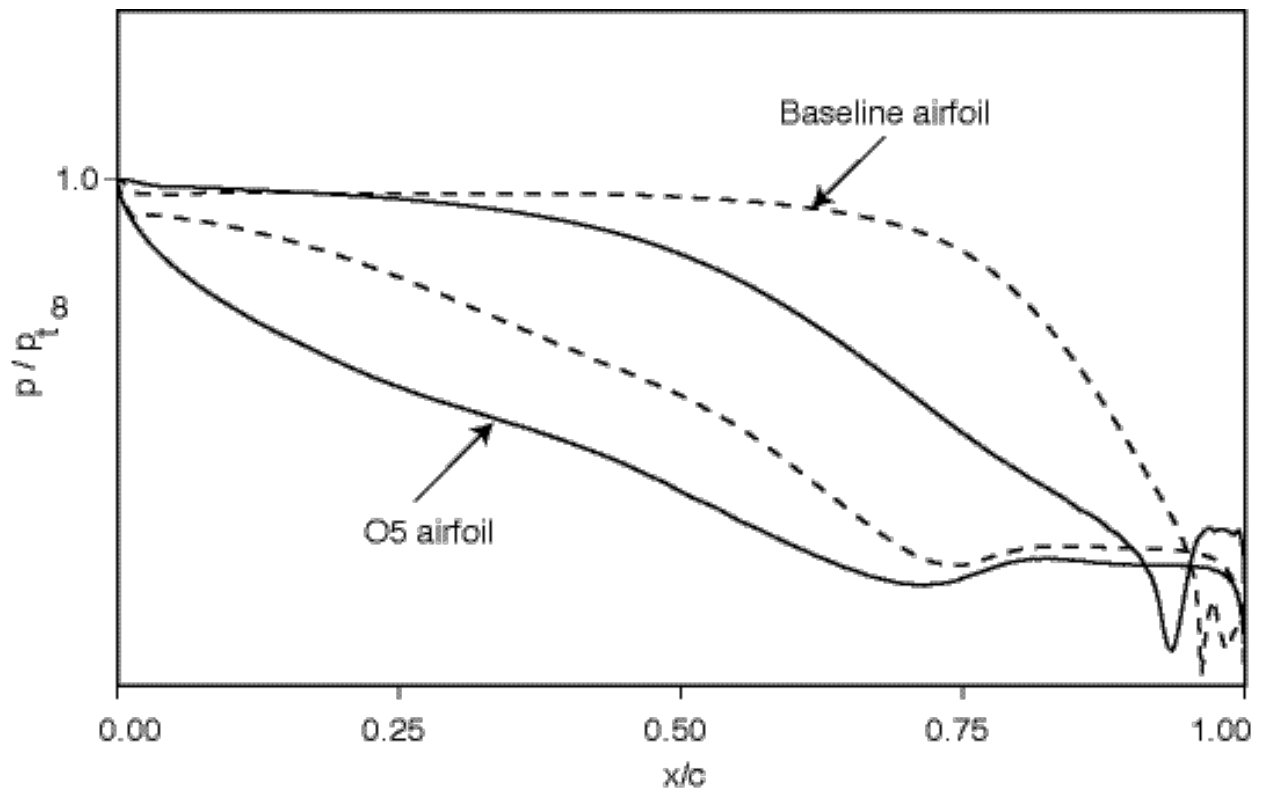
Figure 2. Distribution of the time-averaged surface pressure, baseline and O5 airfoils.

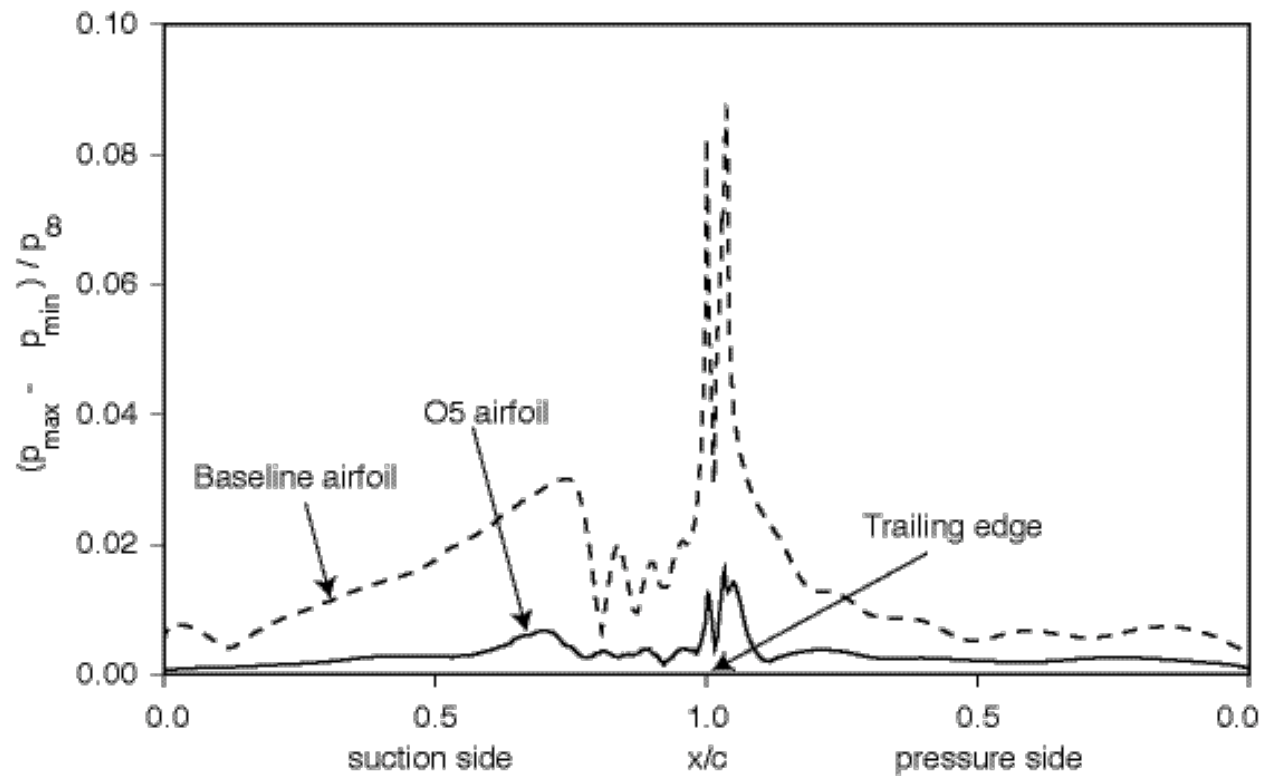American Institute of Aeronautics and Astronautics

Figure 3. Distribution of the unsteady surface pressure amplitude, baseline and O5 airfoils.
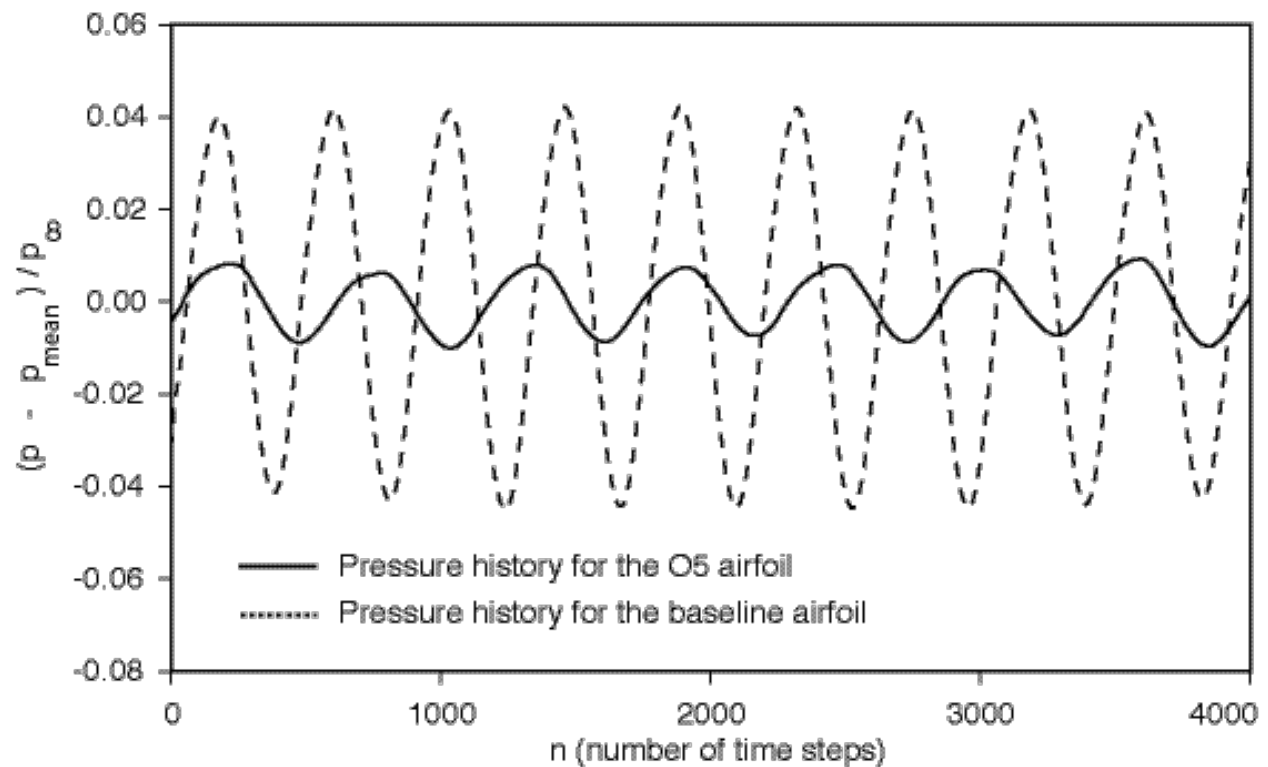
Figure 4. Time-variation of pressure at the point of maximum amplitude, baseline and O5 airfoils.
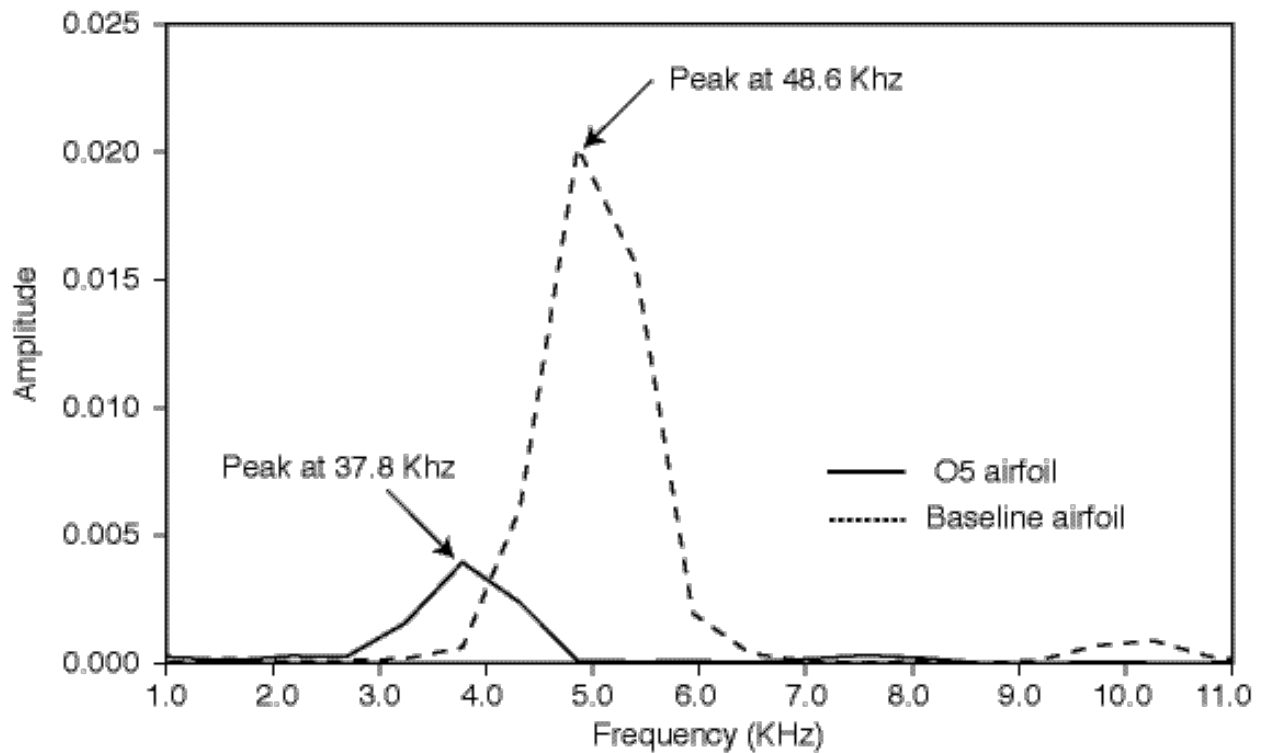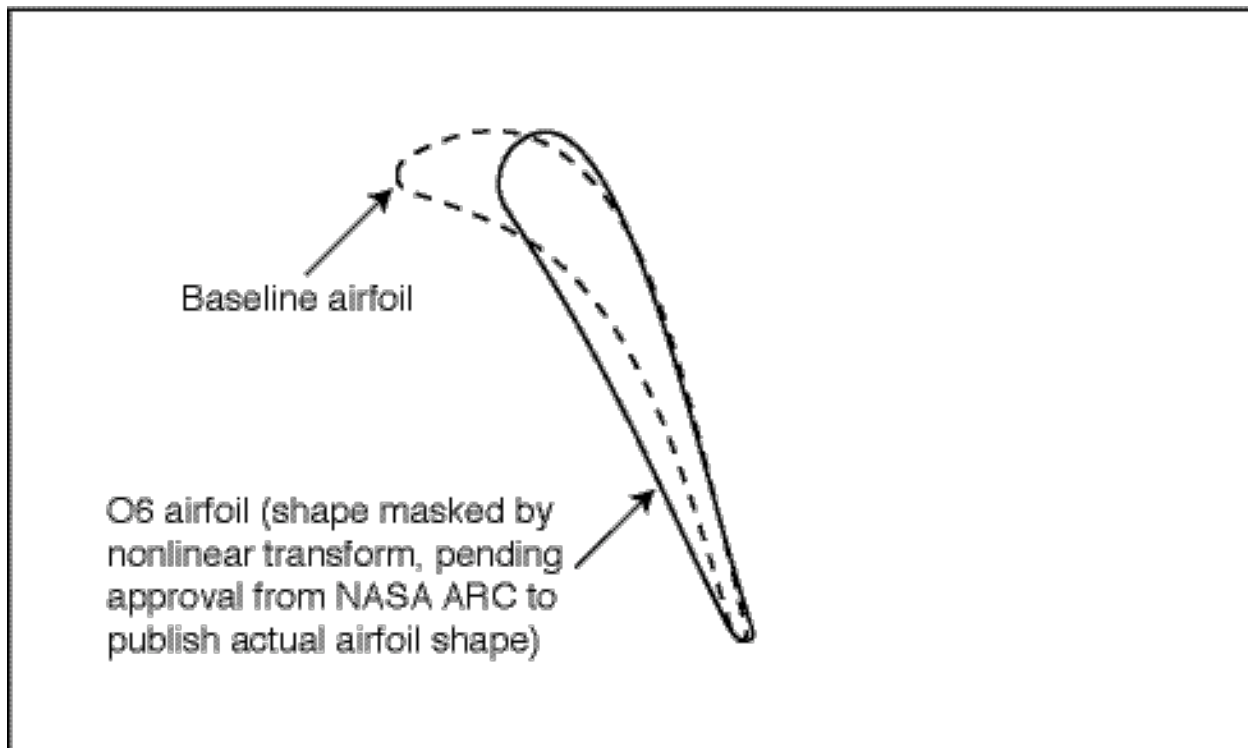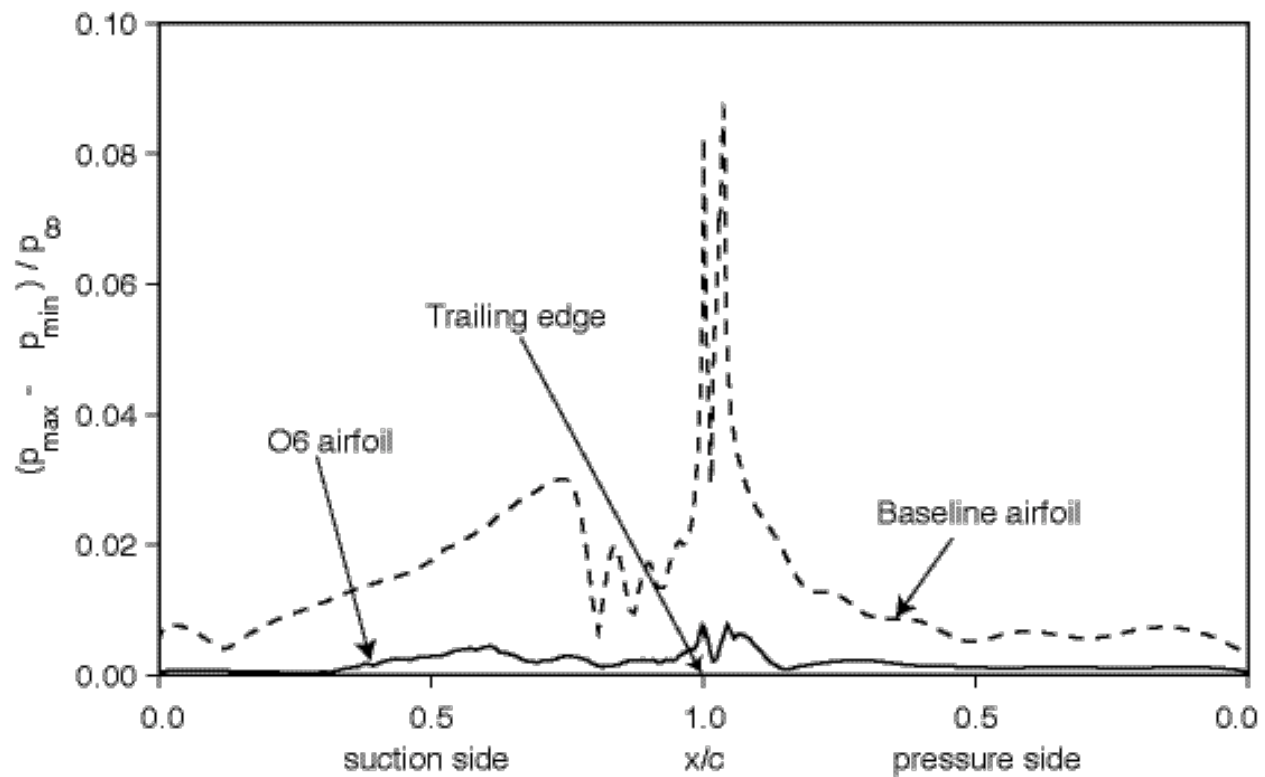
American Institute of Aeronautics and Astronautics

Figure 5. Spectral analysis of the pressure variation at the point of maximum amplitude, baseline and O5 airfoils.

Figure 6. A comparison of the baseline and O6 airfoil shapes.
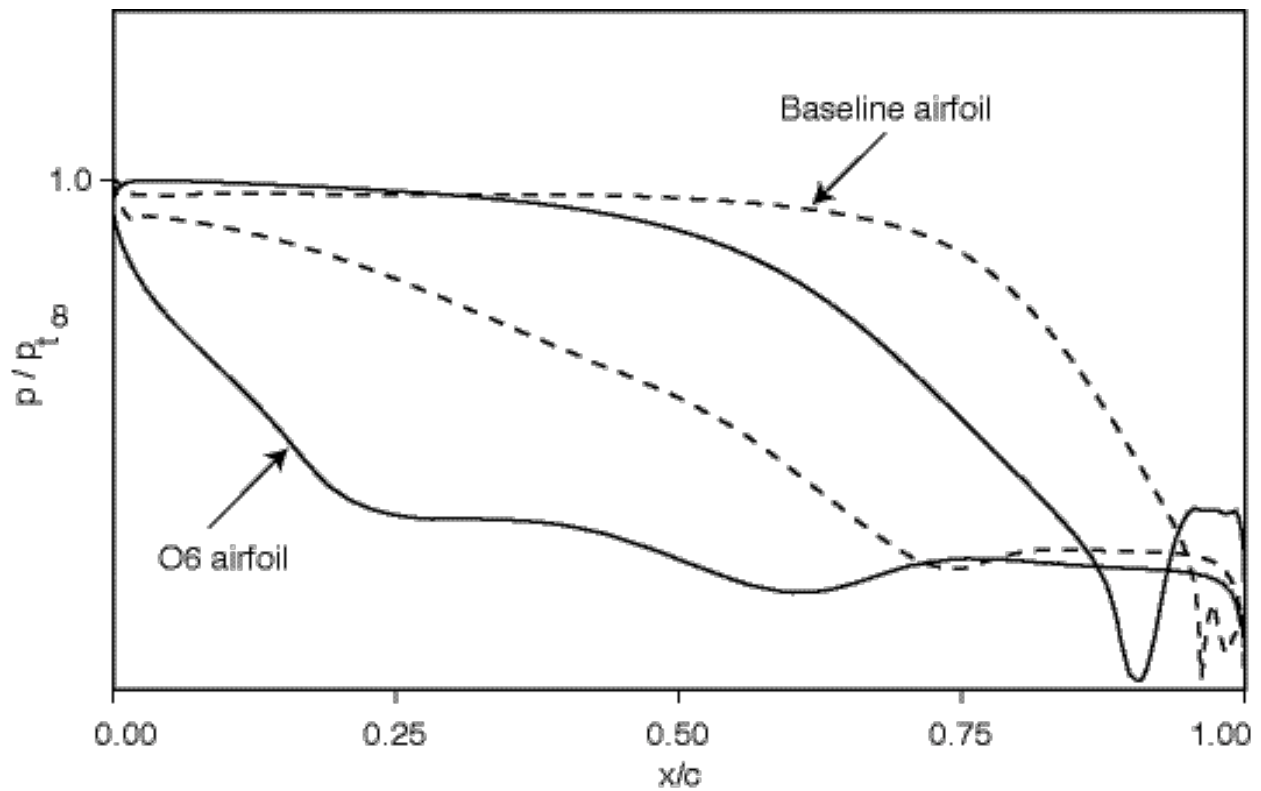
Figure 7. Distribution of the time-averaged surface pressure, baseline and O6 airfoils.

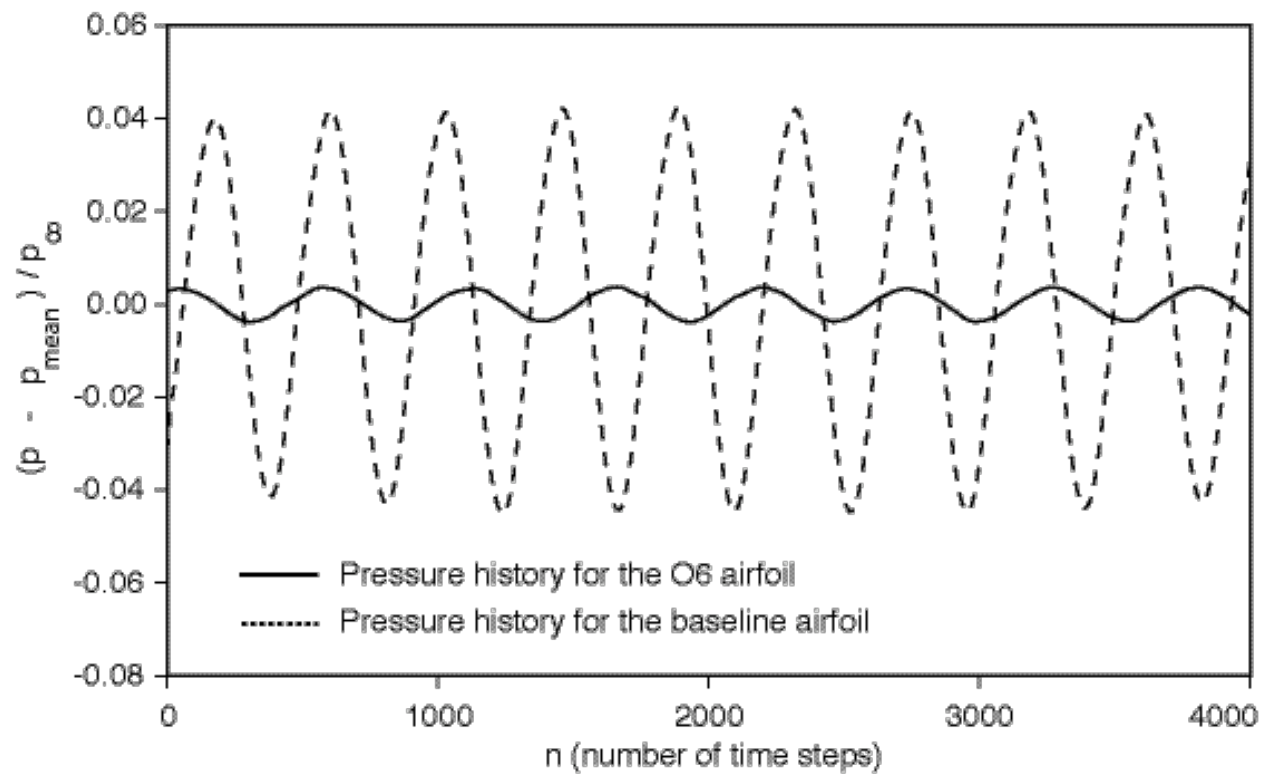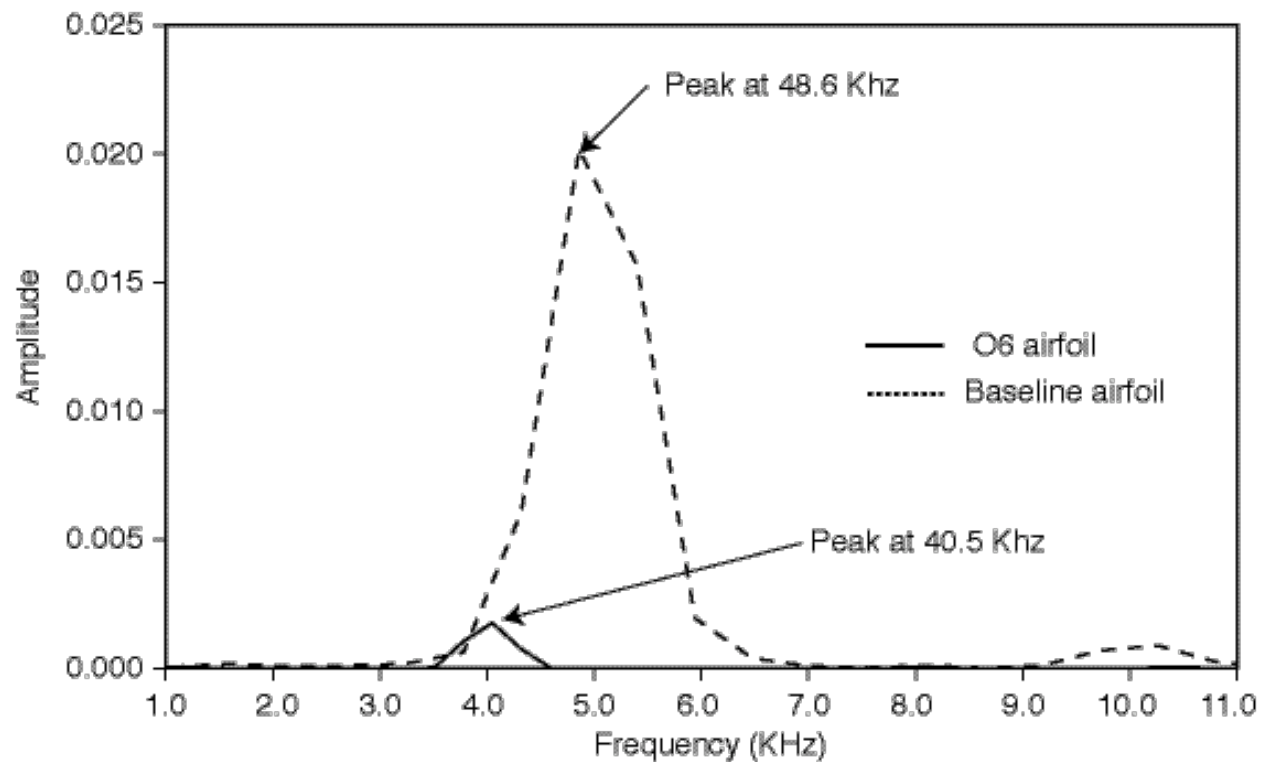Figure 8. Distribution of the unsteady surface pressure amplitude, baseline and O6 airfoils.

American Institute of Aeronautics and Astronautics

Figure 9. Time-variation of pressure at the point of maximum amplitude, baseline and O6 airfoils.

Figure 10. Spectral analysis of the pressure variation at the point of maximum amplitude, baseline and O6 airfoils.
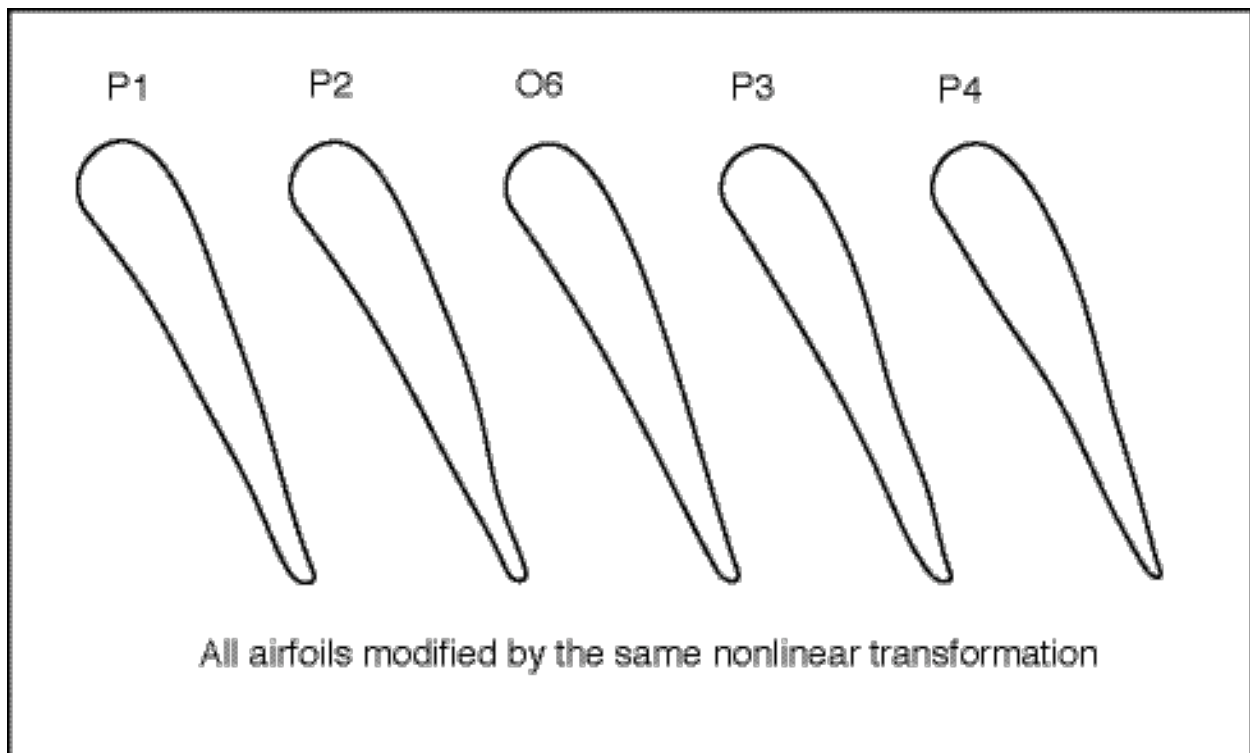
Figure 11. A comparison of the O6 airfoil and its random perturbations.
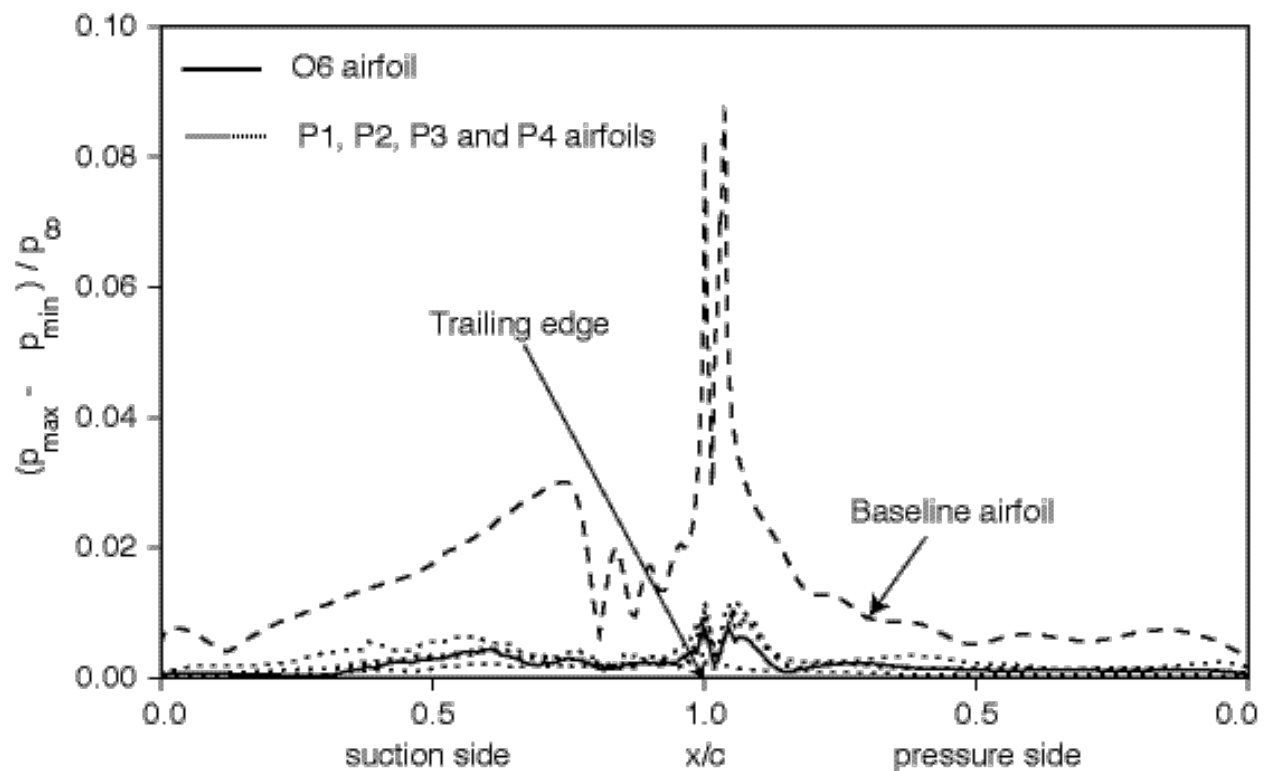

Figure 12. Distribution of the unsteady surface pressure amplitude, O6 airfoil and its random perturbations.

American Institute of Aeronautics and Astronautics